Nanoscale Advances

ROYAL SOCIETY OF CHEMISTRY

REVIEW

View Article Online
View Journal | View Issue

Cite this: *Nanoscale Adv.*, 2020, **2**, 5090

Inorganic–organic core/shell nanoparticles: progress and applications

Viola Chiozzi and Filippo Rossi *

In recent decades a great deal of research has been dedicated to the development of core–shell nanoparticles (NPs). We decided to focus our attention on NPs with inorganic cores and organic shells and divide them by area of application such as electrical applications, drug delivery, biomedical applications, imaging, chemistry and catalysis. Organic shells, consisting in most cases of polymers (natural or synthetic), proteins or complex sugars, can improve the performance of inorganic NPs by enhancing their biocompatibility, acting as anchor sites for molecular linkages or protecting them from oxidation. Moreover, suitable design of the shell thickness can improve the chemical and thermal stability of NPs together with the possibility of tuning and controlling the release of molecules from the core. In the future new discoveries will guarantee improvement in the properties of NPs, synthesis, and applications of this class of nanomaterials that are constantly evolving.

Received 21st May 2020
Accepted 1st August 2020

DOI: 10.1039/d0na00411a

rsc.li/nanoscale-advances

Introduction

Nanomaterials represent, by definition, components with dimensions within the nanometer scale, *i.e.* ≤100 nm. The applications of nanomaterials and nanoparticles in particular can be found in the vast field of science and technology and can be divided into many subcategories such as electronics, chemistry, physics, pharmaceutical, biomedical, agricultural and environmental. The transition from micro to nanoscale brings about important changes in chemical and physical properties, due to the fact that, thanks to the smaller size and higher surface to volume ratio, the surface atoms prevail over those in the inner part.[1,2] The synthesis techniques can be categorised into three wide groups: (1) condensation from vapour, (2) synthesis by chemical reaction, and (3) solid-state processes, such as milling. Using these methods, it is possible to produce

Department of Chemistry, Materials and Chemical Engineering "Giulio Natta", Politecnico di Milano, via Mancinelli 7, 20131 Milan, Italy. E-mail: filippo.rossi@polimi.it; Fax: +39-223993180; Tel: +39-223993145

Viola Chiozzi received her BSc degree from the University of Pisa in chemical engineering in 2017. She then obtained her MSc degree from Politecnico di Milano in chemical engineering in 2019. At the beginning of 2019 she joined the group of Prof. Filippo Rossi working on polymer-based drug delivery systems and spent 6 months at ETH Zurich under the supervision of Prof. Mark Tibbitt. From 2020 she has been a Junior Research Associate at the Department of Chemistry, Materials and Chemical Engineering "Giulio Natta" working on core–shell inorganic–organic nanoparticles for environmental and biomedical applications.

Filippo Rossi received his MSc and then PhD in chemical engineering from Politecnico di Milano in 2007 and 2011 respectively. Then he spent research periods at Uppsala University (2012) and Mario Negri Institute for Pharmacological Research (2013–2015) as a PostDoc and Keio University (2018) as a Visiting Associate Professor. In 2015 he joined the Department of Chemistry, Materials and Chemical Engineering "Giulio Natta" of Politecnico di Milano as an Assistant Professor and from 2019 he has been working as an Associate Professor of Applied Physical Chemistry. His group's research program is focused on developing novel technologies to solve problems associated with health and the environment using functionalized polymers in bulk and colloidal forms.

not only the classic monomaterial structure but also other kinds of nanoparticles such as coated or hybrid types. Depending on the aim, they can also be hydrophilic or hydrophobic. Since the nineties, thousands of published papers regarding these topics have appeared in the scientific world and the "core/shell"[3–5] terminology was adopted after the development of multilayer semiconductor nanoparticles. With the advent of new technologies, new characterisation techniques have properly determined the traits of these new nanostructures. New synthesis methods have made it possible to produce them not only in a spherical shape but also in a range of other shapes such as a cube,[6–13] prism,[14,15] hexagon,[6,7,16–18] octahedron,[10,12] disk,[19] tube,[20–23] wire[20,24–28] and others, considering also the fact that the shape can influence the properties of the particle, for example the catalytic activity,[12,29–31] optical[32,33] and electrical[34,35] properties, and coercivity of magnetic nanocrystals, that depend on anisotropy effects.[11,36]

Core/shell nanoparticles can be categorised considering the two or more multiple materials of the core or the bulk of the particle. Due to the enormous variety of materials and elements present on the Earth, the combinations of them could be impossible to list. For this reason, it seems more appropriate to classify core/shell nanoparticle materials into organic and inorganic substances. In this case, there can be four combinations considering the core and the shell: inorganic/inorganic, inorganic/organic, organic/inorganic, and organic/organic. Varying the materials, it is possible to tune the properties and vary the core to shell ratio.[37] The coating in general can bring advantages such as less cytotoxicity, increase in bio- and cyto-compatibility, dispersibility, and chemical and thermal stability,[2,38] but also makes it possible to control the release of substances from the core for example. The uses investigated by researchers range from biomedical,[39–41] catalysis,[42,43] electronics,[44] and imaging[44–47] to controlled and targeted drug delivery.[48–50] In our work, we focus our attention on the combination of inorganic cores and organic shells. Organic shells, made in most cases of polymers, carbonaceous substances, long-chain acids, cellulose, proteins, complex sugars and so on, enhance the bio- and cyto-compatibility,[2,38] especially for those applications that involve the human body environment. In addition, they protect and guarantee the oxidative stability of the metal core for example. Moreover, in many cases they act as anchor sites for additional molecular linkages. Control of the coating and its thickness during the synthesis process is closely related to the resulting chemical and physical properties of the nanoparticle. The aim of this review is to point out the possible industrial applications of core/shell nanoparticles in different industrial fields to give a broad overview of the different possibilities behind this approach.

Electrical and magnetic applications of core/shell nanoparticles

Inorganic–organic core/shell nanoparticles are also widely investigated for their electrical and magnetic properties. The most used bulk materials for magnetic applications are Fe_3O_4 (ref. 51 and 52) and $MnFe_2O_4$,[53] while for electrical applications we have TiO_2,[54,55] SnO_2,[56] Ag,[57,58] Au,[59] S,[60] $BaTiO_3$,[61] and ZnO.[62] Coating materials used for nanoparticles include polystyrene (PS),[53,54,59,62] polyaniline (PA),[51] oleic acid, graphene,[56] polyvinylpyrrolidone (PVP),[57] polyvinyl acetate (PVA), paraffin, poly(3,4-ethylenedioxythiophene) (PEDOT),[60] hyperbranched aromatic polyamide (HBP),[61] poly(methylmethacrylate) (PMMA),[61] polyethylene-based and polystyrene-based polymers and polyisobutylene.[52] These kinds of materials have peculiar properties that enable them to be used in displays, batteries, optical sensors and magnetic imaging.[51–62] In Table 1 a summary of their use and the nature of the core and shell are presented.

Magnetic nanoparticles

An iron oxide core is very widely used and can be coated with polyaniline, polyisobutylene, polyethylene-based polymers such as poly(ethylene-*graft*-tetraethylenepentamine maleimide) (PE-*g*-TEPA) and polystyrene-based polymers such as poly(styrene-

Table 1 Electrical applications of core–shell NPs

Core@shell material	Application	Reference number
Fe_3O_4@polyaniline	Electric and ferromagnetic	51
$Fe(CO)_5$@polyisobutylene or polyethylene or polystyrene	Electric and ferromagnetic	52
$MnFe_2O_4$@polystyrene	Data storage and MRI contrast enhancement	53
TiO_2@polystyrene	Electric	54
TiO_2@paraffin	Electric	55
SnO_2@graphene	Anode material for lithium ion batteries	56
Ag/polyvinylpyrrolidone and polyethylene glycol	Electric	57
Ag/gelatin and propylene glycol	Electric	58
Au@polystyrene	Organic light-emitting diodes (OLEDs) and organic photovoltaics (OPVs)	59
S@poly(3,4-ethylenedioxythiophene)	Cathode material for lithium/sulphur batteries	60
$BaTiO_3$@poly(methyl methacrylate)	Electric	61
ZnO@polystyrene	Transparent electronics, ultraviolet (UV) light emitters, piezoelectric devices, chemical sensors, and spin electronics	62

graft-tetraethylenepentamine) (PS-*g*-TEPA) and poly(styrene-*block*-tetraethylenepentamine) (PS-*b*-TEPA). Fe_3O_4-polyaniline, obtained by emulsion polymerisation by Deng, J. *et al.*[51] exhibits electrical and ferromagnetic properties. The core–shell structure has an average diameter of 80 nm, with the Fe_3O_4 core having 20–30 nm average size and a polyaniline shell that provides conductive features. Burke, N. A. D. *et al.*[52] synthesised particles by thermal decomposition of iron pentacarbonyl in the presence of ammonia. Using polyisobutylene- and polyethylene-based dispersants they obtained more uniform particle sizes. The former have a diameter range from 8 to 20 nm, with a core diameter between 3 and 14 nm, while the latter have a diameter of 16 nm, with a core diameter of 8.5 nm. With polystyrene-based dispersants, large particles which were made intricate by the aggregation of smaller particles are formed with a diameter range of 24–45 nm and core diameter of 18 to 40 nm. The dimensions are affected by the polymer molecular weight, even if it does not follow a precise correlation. Combinations leading to complex particles are caused by a divergence between the solubility parameters of the dispersant and the reaction solvent. Particle size has a marked influence on the magnetisation grade: samples with larger particles showed higher magnetisations due to the higher iron content.

$MnFe_2O_4$ has been used by Vestal, C. R. *et al.*[53] as a bulk magnetic material with a polystyrene shell. The cores were separately prepared by a reverse micelle microemulsion procedure and then coupled with the polymer by atom transfer radical polymerisation. The nanoparticles have a diameter less than 15 nm, with a core of 9.3 ± 1.5 nm and shell dimension of 3.4 ± 0.8 nm. After coating, a decrease in coercivity was observed which is coherent with the decrease of magnetic surface anisotropy upon the polymer coating. In any case, these composites can be used for specific applications, for instance in data storage and MRI contrast enhancement.

Conductive nanoparticles

Polystyrene (PS) has been found to be largely used as a coating material in nanocomposites for electrical applications.

ZnO as a core material has been investigated by Liu P. *et al.*[62] It has certain features that permit its use in transparent electronics, ultraviolet (UV) light emitters, piezoelectric devices, chemical sensors, and spin electronics. A microemulsion polymerisation method was used to coat the ZnO nanoparticles, with oleic acid modified zinc oxide (OA-ZnO) nanoparticles as seeds, and potassium persulphate (KPS) as an initiator in water. The average core + shell size is around 300 nm, considering a core diameter of 20–80 nm.

Gold–polystyrene nanoparticles have been studied by Kim, T. *et al.*[59] as nanostructures for organic light-emitting diodes (OLEDs) and organic photovoltaics (OPVs). The PS shell is used to ensure stability and protection of the metal core that provides the plasmonic effect. This type of NP could effectively control the excitons in the emitting layer of OLEDs (or the active layer of OPVs) and prevent them from being quenched on the surface of the metal core, also varying the thickness of the shell.

TiO_2 as an inorganic oxide material core has been coupled with PS by Ashok Maliakal *et al.*[54] The high dielectric constant *K* core offers high capacitance and was applied in capacitors presenting up to a 3.6 times enhancement in *K* as compared to PS at 18.2 volume % loading. The values of *K* fluctuate between 9.4 and 8; the thinner the polymer layer is, the higher the *K* value. The flexible shell provides the material with good dispersability and film-forming properties. TiO_2–PS nanocomposites have been found to be of cylindrical shape, 19 ± 5 nm long and 3.4 ± 1 nm wide. Titanium oxide has been covered by Balamurugan Balasubramanian *et al.*[55] with paraffin to improve its dielectric properties. Indeed, the dielectric constant reaches a value of 58, with no organic shell, and for example, 11 with a layer of 2 nm. To produce spherical and monodisperse nanoparticles, a plasma-condensation-type cluster-deposition method and thermal evaporation source are used. The average core size is 13.4 nm. The thickness of the nano-shells is controlled accurately by varying the evaporation rate of the paraffin. Still on the subject of the inorganic core and organic shell, in the research of Xie, L. *et al.*[61] a nanocomposite consisting of a $BaTiO_3$ core and a double organic shell is described; the first material is hyperbranched aromatic polyamide (HBP) and the second outer shell is poly(methyl methacrylate) (PMMA), as synthesised in Fig. 1. Compared with the traditional solution of barium titanate (BT) covered with PMMA, the core@double-shell structured BT@HBP@PMMA nanocomposites shown in Fig. 1 have a higher dielectric constant and lower dielectric loss. The dielectric constant values range from 9.28 for BT@HBP@PMMA-1, that has a MMA to BT@HBP-Br feed ratio of 5.0 to 39.3 for BT@HBP@PMMA-4, with a MMA to BT@HBP-Br feed ratio of 1.0, reaching a value of 130 if the sample is produced with the same ratio but *via* a solution blending method. In any case for this last sample, the electric losses are higher than for the previous one.

Silver has also been used as a bulk material in the studies of Dhakal, T. R. *et al.*[57] and Wu Songping.[58] The first group of researchers used different combinations of polyvinylpyrrolidone (PVP) and polyethylene glycol (PEG) as coating

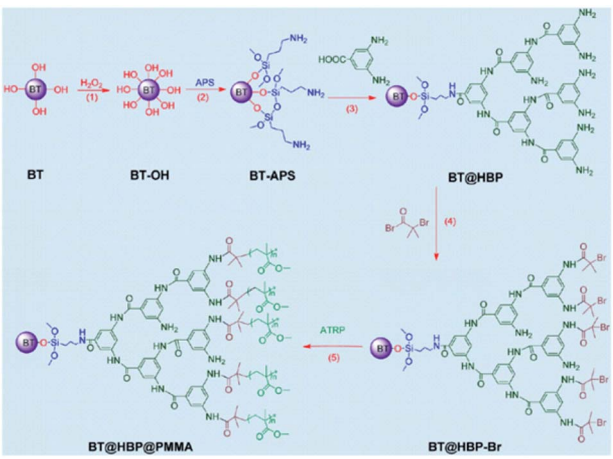

Fig. 1 BT@HBP@PMMA nanocomposite structure. Reprinted with permission from ref. 61. Copyright 2013 American Chemical Society.

polymers, and investigated the effects of varying the two polymer ratios on NP dimensions, shape and thermal stability. The molecular weight of PVP used is 40 000 and that of PEG is 1000. It has been demonstrated that the thermal stability of the nanocomposite deteriorates by as much as 75 °C in the presence of low PEG concentration ($x \leq 0.6$) and is enhanced by around 45 °C at higher PEG concentration ($x > 0.6$). In the presence of pure PVP and PEG, silver NPs favour a spherical shape with an average diameter of 50 nm and 40 nm, respectively. Since PVP is an amorphous polymer having a higher free volume, it permits easy diffusion of silver ions therefore allowing growth of larger silver NPs. Its cross-linking with PEG reduces the overall free volume of the polymer. The low diffusion length and rapid reduction of silver ions lead to arrested growth of silver NPs in an Ag–PVP–PEG nanocomposite. On the other hand, the research of Wu Songping[58] focuses on the preparation of conductive silver powder using gelatin and propylene glycol (PG) as surfactants to synthesise two different samples of Ag particles of 1–2 μm size. It has been seen very clearly that the sheet resistivity of the PG film is lower than that of the gelatin film.

Inorganic core–organic shell nanoparticles and composites have been investigated also as potential anode and cathode materials for lithium batteries

Du, Z. *et al.*[56] have synthesised a SnO_2/graphene nanocomposite for application as an anode material for lithium ion batteries. The electrochemical performance of the SnO_2/graphene nanocomposite as an anode material has been proved by galvanostatic charge/discharge cycling. The SnO_2/graphene nanocomposite exhibited a reversible capacity of 665 mA h g^{-1} after 50 cycles. TEM analysis confirmed the uniform attachment of SnO_2 nanoparticles of 2–4 nm diameter on the graphene nanosheet matrix. On the other hand, nanoparticles made of sulphur with a diameter of 10–20 nm have been coated with conducting poly(3,4-ethylenedioxythiophene) (PEDOT) using a procedure described in the work of Chen, H. *et al.*[60] The research team investigated the application of this type of nanoparticle as a cathode material for lithium/sulphur batteries. They found that the core/shell nanoparticles show an initial discharge capacity of 1117 mA h g^{-1} and a stable capacity of 930 mA h g^{-1} after 50 cycles.

Drug delivery applications

Core–shell nanoparticles are widely used in the field of controlled drug delivery, and some of the applications that are going to be described in this section will be mentioned subsequently because several combinations of materials can be used for many other purposes. For the inorganic core, reconnecting with the previous section, magnetic materials such as magnetite[63–66] and cobalt[63] are investigated. Silica[67–71] has also been analysed in many scientific articles; gold[72] and upconversion luminescent nanoparticles (UCNPs)[73] and ZnO[74] have been found in use for this pharmaceutical application. As coatings, poly(ethylene oxide) with poly(propylene oxide),[63] poly(D,L-lactide-*co*-glycolide) (PLGA),[64] polydopamine,[65] poly(*N*-isopropylacrylamide-*co*-methacrylic acid) (P(NIPAM-*co*-MAA)),[67] coordination polymers,[68] poly(L-lysine),[69] grafted poly(g-benzyl-L-glutamate) (PBLG) with poly(3-carbobenzyloxy-L-lysine) (PZLL) and *S-tert*-butyl protected polycysteine (PtBLC),[70] dextran,[71] functionalised PEG,[72] and metal–organic framework (MOF) structures based on iron(III) carboxylate materials were used.[73] In Table 2 a summary of their use and the nature of the core and shell are presented.

Magnetite core

The magnetite core is widely used in drug delivery devices due to its biocompatibility and stability in biological systems. Chen, S. *et al.*[63] covered the magnetite core with the poly(ethyleneimine)-modified poly(ethylene oxide)-poly(propylene oxide)-poly(-ethylene oxide) (PEO-PPOPEO) block copolymer, which consists of hydrophilic PEO sections and hydrophobic PPOsections. The NPs have a ~20 nm diameter magnetite core and an ~40 nm hydrodynamic diameter. The system they synthesised exhibits

Table 2 Drug delivery applications of core–shell NPs

Core@shell material	Application	Reference number
Fe_3O_4@poly(ethyleneimine)-modified poly(ethylene oxide)-poly(propylene oxide)-poly(ethylene oxide) (PEO-PPOPEO) block copolymer	Drug delivery devices	63
Fe_3O_4@poly(D,L lactide-*co*-glycolide)	Magnetically guided drug delivery	64
Fe_3O_4@polydopamine	Drug carrier, catalyst support and carbon adsorbent	65
Fe_3O_4@poly(*N*-isopropylacrylamide-acrylamide-allylamine)	Magnetically guided drug delivery	66
SiO_2 + Fe_3O_4@poly(*N*-isopropylacrylamide-*co*-methacrylic acid)	Controlled drug release	67
SiO_2@polymer-1,4-bis(imidazol-1-ylmethyl)benzene	Controlled drug release	68
SiO_2@poly(L-lysine)	Delivery of antisense oligonucleotides	69
SiO_2@poly(g-benzyl-L-glutamate), poly(3-carbobenzyloxy-L-lysine), and *S-tert*-butyl protected polycysteine	Drug delivery application in response to a targeted pH trigger	70
SiO_2@chitosan	pH-responsive drug delivery system	71
Metal (Au, Pt, Pd)@polyethylene glycol conjugated ligands	Drug and gene delivery	72
$NaYF_4$:Yb^{3+}/Er^{3+}@metal organic framework	Targeted drug delivery and cell imaging	73
ZnO@polymer quantum dots	pH triggered drug delivery system	74

a temperature-responsive volume-transition property. Dynamic light scattering analysis results indicated that their average hydrodynamic diameter is reduced considerably from 45 to 25 nm. The saturation magnetisation value is 51.34 emu g^{-1} at 25 °C. The uptake and release of both hydrophobic and hydrophilic model drugs are appropriately regulated by shifting the transient opening and closing of the polymer shell at distinct temperatures. The nanoparticles show good aqueous stability, monodispersity and also superparamagnetism.

Liu, X. *et al.*[64] synthesized high magnetisation, biodegradable/biocompatible polymer-coated magnetic nanospheres for magnetically guided drug delivery. The coating is made of poly(D,L-lactide-*co*-glycolide) (PLGA). Magnetic particles are prepared by a modified single oil-in-water emulsion–solvent evaporation technique. The content of magnetite encapsulated is around 84 wt% with a mean sphere diameter of 360–370 nm.

The saturation magnetisation values of the magnetite are 26–40 emu g^{-1}, which increase with magnetite loading.

Liu, R. *et al.*[65] have synthesized multipurpose core–shell Fe_3O_4–polydopamine (PDA) nanoparticles as drug carriers, catalyst supports and carbon adsorbents. They experimented with Fe_3O_4@PDA NPs for controlled drug release in a pH-sensitive way *via* reversible bonding between catechol and boronic acid groups of PDA and the anticancer drug bortezomib. The NP shape is spherical and uniform, with a diameter of ~240 nm considering the core plus 20 nm more including the organic shell.

Rahimi, M. *et al.*[66] evaluated novel polymer-coated magnetic nanoparticles for controlled drug delivery. The nanostructure consists of a poly(*N*-isopropylacrylamide-acrylamide-allylamine) coating and a silane-coated magnetite core. Spherical core–shell nanoparticles with a diameter of 100 nm exhibit significantly lower systemic toxicity than bare magnetite NPs. Doxorubicin encapsulation efficiency is demonstrated to be 72%, and a significantly higher doxorubicin release at 41 °C compared with 37 °C has been recorded, demonstrating their temperature sensitivity.

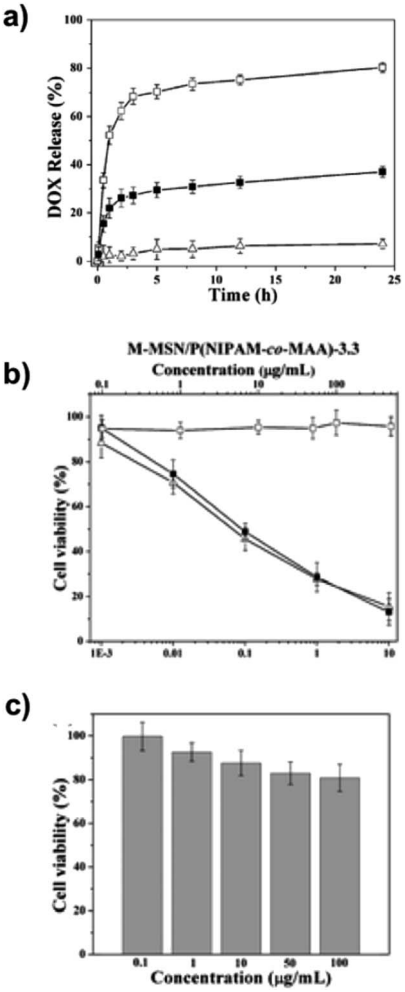

Fig. 2 (a) pH-dependent DOX release profiles of DOX@M-MSN–P(NIPAM-*co*-MAA)-3.3 at (□) pH 5.0, (■) pH 6.5 and (Δ) pH 7.4 in the same NaCl concentration (0.15 M) at 37 °C. (2) Cell survival assay. (b) HeLa cells: (□) blank M-MSN–P (NIPAM-*co*-MAA)-3.3, (■) DOX@M-MSN–P(NIPAM-*co*-MAA)-3.3, and (Δ) free DOX. (c) HEK 293 cells exposed to blank M-MSN–P(NIPAM-*co*-MAA)-3.3. Adapted with permission from The Royal Society of Chemistry.[67]

Silica core

Baisong Chang *et al.*[67] have investigated the thermo and pH dual response of polymer shell coated, magnetic mesoporous silica nanoparticles for controlled drug release applications. The microspheres were prepared, in the presence of Fe_3O_4 nanoparticles, based on magnetic mesoporous silica nanoparticles (M-MSN) with poly(*N*-isopropylacrylamide-*co*-methacrylic acid) (P(NIPAM-*co*-MAA)) as the organic coating *via* precipitation polymerisation. The molar ratio of MAA to NIPAM and the concentration of NaCl regulate thermo/pH-coupling sensitivity and the volume phase transition. The encapsulation efficiency is seen to be about 91.3% under alkaline conditions. The DLS analysis revealed a diameter of 190 nm for M-MSN at 25 °C and 410 nm for MMSN–P(NIPAM-*co*-MAA) at 55 °C. The saturation magnetisation value is 1.5 emu g^{-1} for M-MSN–P(NIPAM-*co*-MAA). Increasing the pH value led to a significant increase in the volume phase transition temperature and no cytotoxicity was found, as shown in Fig. 2.

Xing, L. *et al.*[68] investigated the pH response of mesoporous silica core nanoparticles (MSNs) too. The shell, instead, consists of coordination polymer 1,4-bis(imidazole-1-ylmethyl)benzene (BIX) grown on the MSN surface, building the MSN–NH_2–TPT@BIX–Zn structure with an average diameter of about 100 nm. The release amounts of topotecan (TPT) and topoisomerase I inhibitors, from a MSN–NH_2–TPT@BIX–Zn system suspended in solutions at pH 7.4 are seen to be less than 12% over 24 hours, implying that coordination polymer coated MSNs are stable for a long time under physiological conditions.

Zhu, S.-G. *et al.*,[69] with their work based on poly(L-lysine) (PLL)-modified silica nanoparticles for the delivery of antisense oligonucleotides, demonstrated the ability of PMS-NP (PLL modified silica nanoparticles) to bind and protect antisense oligonucleotides (ODNs).

Polypeptide core–shell silica nanoparticles have been analysed by Borase, T. *et al.*[70] to synthesize a pH-responsive

inorganic–organic hybrid material, using a ring opening polymerisation method with *N*-carboxyanhydride (NCA). Poly(g-benzyl-L-glutamate) (PBLG), poly(3-carbobenzyloxy-L-lysine) (PZLL), and *S-tert*-butyl protected polycysteine (PtBLC) were grafted from the silica core both individually as homopolypeptides and at the same time to form a copolypeptide shell. The selective release of rhodamine B was analysed to prove the potential use of these hybrid nanomaterials for drug delivery application in response to a targeted pH trigger. Furthermore, covalent bioconjugation was shown by attachment of a green fluorescent protein. Reaction temperatures influence the NP dimension and a higher ratio of NCA monomer to silica nanoparticles results in larger functionalised nanoparticles. When the reactions take place at 0 °C a significant increase in hydrodynamic radii from 172 to 236 nm is observed and the ratio was increased from 1 to 3, respectively. At 20 °C a similar increase in hydrodynamic size from 150 nm to 210 nm was observed. Deprotection of the benzyl ester from PBLG grafted silica nanoparticles gives rise to pH-responsive core–shell hybrid nanoparticles. Selective release of rhodamine B was demonstrated when the surrounding solution pH was switched from pH 2 to pH 10.

Amirali Popat *et al.*[71] developed a pH-responsive drug delivery system based on chitosan coated mesoporous silica nanoparticles. Starting from the synthesis of phosphonate functionalised mesoporous silica nanoparticles (MSNs), (MCM-41-PO_3) nanospheres, the phosphoramidate covalent bonding creates a link between phosphonate groups on the surface of the MSNs and amino groups on chitosan. The spherical nanoparticle synthesis is outlined in Fig. 3 with a mean diameter of about 110 nm.

The release of ibuprofen has been investigated and found to be pH dependent through a variation of the charged chitosan shell in the designed pH 4.0–7.4 solution. In an alkaline environment, chitosan forms a gel-like structure which is insoluble and therefore prevents ibuprofen release at pH 7.4. When the pH is below its isoelectric point (6.3), the drug is released due to protonation of the amino group on chitosan.

Other materials

Otsuka, H. *et al.*[72] analysed the scientific research in the field of functionalised poly(ethylene glycol) (PEG) layers as a hydrophilic outer shell for drug and gene delivery through PEG-conjugated ligands with a minimal non-specific interaction with other proteins. By controlling the metal (Au, Pt, Pd) and semiconductor structure precisely through the concept of constructing functionalised PEG layers, nanostructures can be modified to better suit their integration in biological systems. Metal–organic framework (MOF) shell nanocomposites for targeted drug delivery and cell imaging have been studied by Deng, K. *et al.*[73] For the core material they decided to use upconversion luminescent $NaYF_4$:Yb^{3+}/Er^{3+} nanoparticles (UCNPs) that could emit strong green emissions under a 980 nm laser. The MOF structure based on the iron(III) carboxylate material [MIL-100(Fe)] has high porosity and non-toxicity, features that make it suitable as a nanocarrier for drug storage/delivery. Moreover the NPs show pH-sensitive drug release. The average size of UCNPs@MOF NCs in deionized water is 138.8 nm while in a cell culture medium containing fetal bovine serum it is found to be 125.1 nm. In order to enhance the affinity between UCNPs and MIL-100(Fe), polyvinylpyrrolidone (PVP) was capped onto the surface of the UCNP core for the coordination interaction between pyrrolidone rings and Fe^{3+} ions. Biodegradable ZnO@polymer Quantum Dot (QD) core–shell nanocarriers have been synthesised by Zhang, Z. Y. *et al.*[74] for use as a pH triggered drug delivery system. They developed a two-step copolymerisation method for the synthesis of a core–shell ZnO@polymer structure of 3 nm size. The ZnO@polymer QDs are very stable in aqueous solution at pH 7.0, but rapidly decompose from pH 6.0, increasing the drug release. Furthermore, both ZnO and the polymer shell are biodegradable and thus safe for cells.

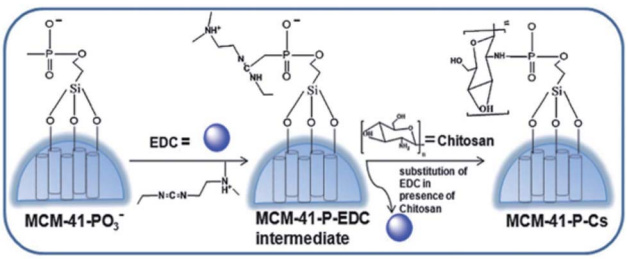

Fig. 3 Schematic procedure of the preparation of chitosan coated mesoporous silica NPs. Reprinted with permission from The Royal Society of Chemistry.[71]

Other biomedical applications

In this field the most investigated possible uses of inorganic–organic core–shell NPs target the treatment of cancers, specific delivery of therapeutics, drug delivery monitoring, biosensors, bioimaging and antibacterial activity. Among the materials used for the core, it is common to find iron oxide,[75–84] gold,[85–87] graphitic carbon nitride (g-C_3N_4),[88] silica[89] and upconversion NPs,[90] while for the organic shell polyethylene glycol,[75,76] proteins[84] such as dextran and albumin,[77] gelatin,[78] curcumin,[79] dopamine-,[83] siloxane-, phosphonate-, carboxyl group-based coatings,[80] polyanilin,[81,85] metal organic frameworks,[88] *N*-halamine,[89] polyvinylpyrrolidone[90] (PVP), polyethylenimine[90] (PEI) and poly(acrylic acid)[90] (PAA) are used. In Table 3 a summary of their use and the nature of the core and shell are presented.

Iron core

By reversible addition–fragmentation chain transfer (RAFT) polymerization, Qin, S. *et al.*[75] have grafted poly(ethylene glycol) monomethacrylate (P(PEGMA)) onto Fe_3O_4 nanoparticles that resist nonspecific protein adsorption. The researchers clearly observed that proteins are adsorbed onto the surface of the naked magnetic nanoparticles (MNPs), while the nonspecific protein adsorption on MNPs is reduced by the P(PEGMA) outer layer. The mean diameter of MNPs-P(PEGMA) is about 15.4 ± 5.4 nm. The magnetic saturation value is 49.5 emu g^{-1}, whereas

Table 3 Biomedical applications of core–shell NPs

Core@shell material	Application	Reference number
Fe_3O_4@poly(ethylene glycol) monomethacrylate	Nonspecific protein adsorption	75
Fe_3O_4@poly(ethylene glycol)	Localised hyperthermia treatment of cancers	76
Fe_3O_4@dextran and albumin	Observation of cell–particle interactions through light and fluorescence microscopy, scanning and transmission electron microscopy	77
Fe_3O_4@gelatin + dextran + human serum albumin	Immunogenicity of bioactive magnetic nanoparticles	78
Fe_3O_4@curcumin	Multimodal monitoring and drug targeting to treat tumour cells	79
Fe_3O_4@dopamine + siloxane + phosphonate and carboxyl groups	Targeted carriers for the delivery of drugs and other biomolecules, hyperthermia treatment for cancer therapy, and highly efficient MRI contrast agents	80
Fe_3O_4@polyaniline	Heat activated killing of cancer cells under an AC magnetic field	81
Fe_3O_4@antibodies	Binding of human cancer cells	82
Fe_3O_4@polydopamine	Protein recognition	83
Fe_3O_4@protein sequences	Adaptive chemo-enzymatic microreactors	84
Au@polyaniline	Glucose biosensor	85
Au@amphiphilic polymers	Interaction with proteins and cells	86
Au@plasma-polymerized allylamine	Cancer cell targeting	87
Graphitic carbon nitride (g-C_3N_4)@zeolitic-imidazolate framework-8 (ZIF-8)	Photo-chemo combination therapy with a pH-sensitive release delivery profile	88
SiO_2@*N*-halamine	Antibacterial performance against both Gram-positive bacteria and Gram-negative bacteria	89
$NaYF_4$:Yb^{3+},Er^{3+} lanthanide-doped@polyvinylpyrrolidone	Two-photon induced NIR live-cell imaging	90
Fe_3O_4@dopamine + siloxane + phosphonate and carboxyl groups	Targeted carriers for the delivery of drugs and other biomolecules	91

for simple MNPs it is 68.9 emu g^{-1}. The work of Zhao, D. L. *et al.*[76] highlights the magnetic and inductive heating properties of Fe_3O_4 core/polyethylene glycol (PEG) shell composite nanoparticles. The NPs are prepared by coprecipitation of Fe^{3+} and Fe^{2+} using ammonium hydroxide (NH_4OH) as a precipitating agent. The Fe_3O_4/polyethylene nanostructure presents a core–shell structure with a diameter of 10–40 nm. The saturation magnetisation value is 67.06 emu g^{-1} for Fe_3O_4 nanoparticles and 64.11 emu g^{-1} for Fe_3O_4/PEG. The inductive heat property of Fe_3O_4/PEG composite nanoparticles in an alternating current (AC) magnetic field has been analysed; applying an AC magnetic field for 100 s, the temperatures of physiological saline suspensions containing Fe_3O_4 nanoparticles or Fe_3O_4/PEG composite nanoparticles are 89.2 °C and 72.2 °C, respectively. For this proven activity, the Fe_3O_4/PEG NPs could be useful for localised hyperthermia treatment of cancers. Rana, S. *et al.*[81] have instead used polyaniline shell cross-linked Fe_3O_4 magnetic nanoparticles (PSMNs) for heat activated killing of cancer cells under an AC magnetic field (AMF). The PSMNs are almost spherical in shape with an average size of 65 nm. The saturation magnetisation value was found to be 63.5 emu g^{-1} for PSMNs at 20 kOe. This low value of magnetisation compared to bulk Fe_3O_4 (92 emu g^{-1}) can be due to the combined effect of nano-sized Fe_3O_4 particles (high surface to volume ratio) and robust coating of the nonmagnetic organic material on the surface. Considering the temperature of the magnetic suspension at a concentration of 1 mg ml^{-1} of Fe, it rises to 43 °C (hyperthermia temperature) within 15 min. Moreover, it has been observed that PSMNs have negligible cytotoxicity. The release of drug molecules from doxorubicin-PSMN follows a time-dependent and diffusion-based sustained release profile.

Dextran and albumin have been used as organic shell materials by Berry, C. C. *et al.*[77] to coat iron oxide NPs in order to observe how cells and particles interact by light and fluorescence microscopy and scanning and transmission electron microscopy. The results suggest that the derivatised particles induce modifications in cell behaviour and morphology. Derivatisation of the particles with either dextran or albumin altered the uptake of iron oxide by human fibroblasts, probably through endocytosis, that causes cell death. Although the dextran nanoparticles are also endocytosed causing eventual cell death, the albumin derivatised particles show cell proliferation together with signs of partial endocytosis. Ziv, O. *et al.*[78] proved the immunogenicity of bioactive magnetic nanoparticles, covered with a gelatin (Gel) film that embraces the magnetic core (Gel-MNP), which in turn is coated with dextran (Gel-MNP-Dex) followed by human serum albumin (Gel-MNP-Dex-HSA). The studies reveal that the plasma of nonimmunised mice already includes basal levels of natural antibodies against all of these antigenic components (porcine gelatin, dextran, and HSA) and also demonstrate that the conjugated gelatin is a weak immunogen. The mean diameter of the NPs is 17 ± 3 nm, as shown by TEM analysis, while the saturation magnetisation value is 41 emu g^{-1}. A magnetofluorescent Fe_3O_4–curcumin

nanostructure has been synthesised by Tran, L. D. *et al.*[79] for multimodal monitoring and drug targeting to treat tumour cells. The shell consists of chitosan (CS) or oleic acid (OL) and entrapped curcumin (Cur), serving the dual function of a naturally autofluorescent dye and anti-tumour model drug. The particles have a mean diameter of 300 nm and 500 nm for OL–Cur and CS–Cur, respectively. For saturation magnetisation, non-coated Fe_3O_4 NPs have a value of 70 emu g^{-1}, CS-coated Fe_3O_4 fluid (CSF) has 1.225 emu g^{-1} and CSF–Cur has 1.209 emu g^{-1}, with a concentration of Fe_3O_4 estimated as 17.5 and 14.7 mg ml^{-1} respectively. Even though CSF is magnetically stable in distilled water for several weeks, in a physiological solution (1× PBS, pH 7.4) the stability of CSF and CSF–Cur deteriorates drastically after a few hours, whereas the diluted OL-coated Fe_3O_4 fluid (OLF) and OLF–Cur still maintained their remarkable stability, at least for 1–2 weeks. The improved stability of OLF over CSF can be justified by the fact that the CS backbone consists of charged groups, making the CS-coated surface charged and therefore pH sensitive in a more pronounced way than that in OLF/OLF–Cur systems. Zhou, L. *et al.*[80] investigated core–shell structured iron oxide hybrid nanoparticles, consisting of Fe_3O_4 as a core and organic coatings based on dopamine, siloxane, phosphonate and carboxyl groups. Dopamine (DPA) is widely used thanks to the *ortho*-dihydroxyphenyl (catechol) functional group, which firmly coordinates to several inorganic/organic surfaces. Various siloxanes with different terminal groups, such as amino groups, halogens, and methacrylic groups, are on the market. Phosphonate is an effective anchoring agent thanks to the ability of $-PO(OH)_2$ groups to form complex metal ions that are stable even at high temperature. From their research they found that iron oxide nanoparticles (IONPs) can be induced to the target by an external magnetic field, so they can be used as targeted carriers for the delivery of drugs and other biomolecules. In combination with the magnetothermal effect, IONPs can be applied in hyperthermia treatment for cancer therapy. IONPs can also be used as highly efficient MRI contrast agents because they can produce predominantly spin–spin relaxation effects. Due to advances in surface functionalisation technology, specific-site targeting molecules can be linked to the surface of IONPs, and active targeting can be achieved, which can improve the efficiency notably in targeted delivery, hyperthermia and MRI. Surface functionalisation of IONPs can also provide a facile platform for immobilisation and separation of biomolecules that can be used for bio-probe or bio-sensor applications. Regarding inorganic/organic hybrid nanoparticles, Choi, H. S. *et al.*[91] specified that to avoid non-specific background fluorescence and long-term toxicity, they need to be cleared from the body within a reasonable timescale. Xu, H. *et al.*[82] have developed antibody conjugated magnetic iron oxide nanoparticles for cancer cell separation in fresh whole blood. The polymer coated 30 nm iron oxide (IO) was altered with antibodies (Ab) against human epithelial growth factor receptor 2 (anti-HER2 or anti-HER2/neu) forming IO–Ab. HER2 is a cell membrane protein that is over-expressed in several types of human cancer cells. Using an HER2/neu overexpressing human breast cancer cell line, SKBR3 as a model cell, the IO–Ab was used to separate 73.6% (with a maximum capture of 84%) of SK-BR3 cells that were spiked in 1 mL of fresh human whole blood. Under a magnetic field, the NPs capture one cancer cell over 1 00 00 000 normal cells through the binding of IO–Ab on the cell surface. The hydrodynamic size of IO–Ab nanoparticles was 41 nm exhibiting an increase of about 8 nm in diameter.

Zhou, W. H. *et al.*[83] fabricated a mussel-inspired molecularly imprinted polymer by coating superparamagnetic nanoparticles for protein recognition. Self-polymerised dopamine coats the Fe_3O_4 NPs by means of a polymer template: Fe_3O_4 nanoparticles and human haemoglobin are first dissolved in a buffer and then dopamine is added. Fe_3O_4 NPs have a mean diameter of 100 nm and a polydopamine (PDA) coating of 10 nm. Magnetic measurements reveal that Fe_3O_4@PDA NPs have superparamagnetic properties and a saturation magnetisation value of 73.2 emu g^{-1} that permits collection of the NPs using a magnet. The behaviour of proteins on the human haemoglobin (Hb) imprinted Fe_3O_4@PDA NPs exhibits substantial preferential binding of Hb compared to the control group Fe_3O_4@PDA synthesised with no imprinting and it was also proved by using other types of proteins like myoglobin, cytochrome C and horseradish peroxidase (HRP).

Palmiero, U. C. *et al.*[84] have discovered and synthesised adaptive chemo-enzymatic microreactors consisting of inorganic nanoparticles and bio-inspired intrinsically disordered proteins. The magnetic iron inner particle has been functionalised with multi-domain protein sequences, defined as low complexity domains (LCDs) that encode intermolecular interactions, and a globular enzyme. The former are improved in polar amino acids and mediate pi-cation, hydrophobic, and electrostatic interactions. The self-assembly behaviour is due to these charges and interactions and is influenced by the pH and ionic strength. In a pH range of 5 to 9 phase separation occurs and under conditions of low ionic strength, stability is reduced and cluster formation may occur. Analysis with DLS, SEM and TEM has shown a wide size distribution with an average diameter of 52 ± 15 nm. On examining with fluorescence microscopy, it was found that the phosphotransferase enzyme AK activity which catalyses the interconversion of adenine nucleotides has been controlled and it has been observed that the droplet chains locally concentrate the activity of the enzyme. Another subject of investigation was the peroxidase-like catalytic activity of the iron NPs through the reduction monitoring of hydrogen peroxide which was detected. This reaction is commonly used to quantify the concentration of many biomolecules in diagnostics and to produce functional biosensors. In conclusion, it is possible to define these new hybrid structures as open micro-reactors that are able to confine chemical reactions locally and sense the presence of molecules in the surrounding environment.

Gold core

Xian, Y. *et al.*[85] designed a glucose biosensor based on a Au nanoparticles–conductive polyaniline (PANI) nanocomposite. The glucose biosensor shows a linear calibration curve over the range from 1.0×10^{-6} to 8.0×10^{-4} mol L^{-1}, with a slope and

detection limit (S/N = 3) of 2.3 mA M^{-1} and 5.0 × 10^{-7} M, respectively. Au NPs can be loaded onto nanofibres, forming a PANI–metal nanocomposite with diameters between 60 and 80 nm. The amperometric response of glucose at Au NPs–PANI nanocomposite modified biosensors is enhanced about six times compared to simple PANI nanofibre modified biosensors. Hühn, D. *et al.*[86] analysed polymer-coated gold nanoparticles interacting with proteins and cells, focusing on the sign of the net charge. The metallic nanoparticles were modified with amphiphilic polymers to obtain NPs with identical physical properties except for the sign of the charge (negative/positive). The aim of the research was to understand how the surface charge of the nanoparticles interferes with proteins and cells. It has been observed that the uptake rate of NPs by cells is higher for positively than for negatively charged NPs. Moreover, cytotoxicity assays exhibited higher cytotoxicity for positively charged NPs associated with their enhanced uptake. Hydrodynamic diameters of negatively and positively charged NPs were determined to be 14.5 ± 1.0 nm and 10.1 ± 0.6 nm, by DLS, respectively. Marega, R. *et al.*[87] have engineered antibody-functionalised polymer-coated gold nanoparticles targeting cancer cells. Gold nanoparticles (5 nm) coated with plasma-polymerized allylamine are produced through plasma vapour deposition and bioconjugated with a monoclonal antibody targeting the epidermal growth factor receptor, with a loading of about 1.7 nmol mg^{-1}. After doping the gold nanoparticles with radionuclides during plasma vapour deposition, these types of NPs become a very suitable platform for *in vivo* cancer targeting with nanosized multifunctional particles.

Other materials

Chen, R. *et al.*[88] investigated graphitic carbon nitride nanosheet@metal–organic framework core–shell nanoparticles for photo-chemo combination therapy. The nanostructure consists of a zeolitic-imidazolate framework-8 (ZIF-8) as a shell embedded with graphitic carbon nitride (g-C_3N_4) nanosheets as the core and is shown in Fig. 4. Doxorubicin hydrochloride (DOX), an anti-tumour drug, is then loaded with a photodynamic therapeutic (PDT) agent into the ZIF-8 shell of the core–shell nanoparticles. The combination of the chemotherapeutic effects of DOX and the PDT effect of g-C_3N_4 nanosheets can lead to considerably enhanced efficacy. The drug delivery presents a preferred pH-sensitive release profile. Additionally, DOX-loaded g-C_3N_4@ZIF-8 nanoparticles, as a multifunctional nanoscale platform, are effective for dual-colour fluorescence imaging and imaging-guided photo-chemo therapy of tumour cells. The spherical nanoparticles have an average size of about 60 nm.

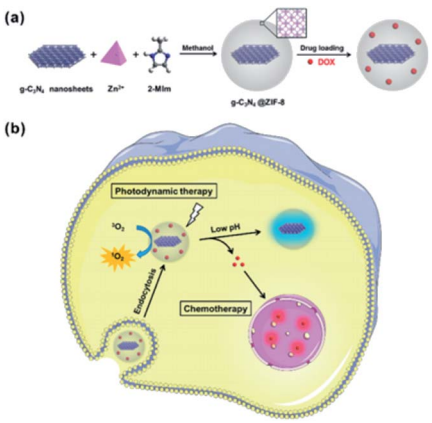

Fig. 4 Illustration of core–shell NPs and (a) their preparation and (b) a proposed mechanism of drug-loaded NPs for fluorescence imaging and combination therapy. Reprinted with permission from The Royal Society of Chemistry.[88]

The enhanced antibacterial activity of *N*-halamine-functionalised silica–polymer core–shell nanoparticles has been proved by Dong, A. *et al.*[89] The synthesised nanostructure exhibits a powerful antibacterial performance against both Gram-positive bacteria and Gram-negative bacteria, and their antibacterial activities are found to be improved compared with that of the silica bulk itself. The possible applications are in the field of medical devices, healthcare products, water purification systems, hospitals, dental office equipment, and food packaging. The size of the nanoparticles, which are spherical, can be varied by changing the quantity of the silica source during synthesis, and is in the range of 220.0–510 nm. Polymeric *N*-halamine is coated onto silica cores *via* copolymerisation with styrene, acrylate acid, methyl methacrylate, and vinyl acetate, respectively. The controllable synthesis of 3-(methacryloxy) propyl trimethoxy silane (MPS) modified silica nanoparticles makes it possible to prepare *N*-halamine-functionalized silica–polymer core–shell nanostructures with different sizes. Due to the particle size effect, the *N*-halamine-functionalised silica–polymer core–shell nanoparticles with a diameter of ~220 nm had better antibacterial activity than the ~510 nm counterparts.

Jin, J. *et al.*[90] analysed polymer-coated $NaYF_4$:Yb^{3+},Er^{3+} lanthanide-doped upconversion nanoparticles for charge-dependent cellular imaging. They used a hydrothermal method to synthesise polyvinylpyrrolidone-coated UCNPs (UCNP-PVP), and then a ligand exchange reaction was performed on UCNP-PVP, with the help of polyethyleneimine (PEI) and poly(acrylic acid) (PAA), to obtain UCNP-PEI and UCNP-PAA. The hydrodynamic diameter of the three polymer-coated UCNPs was measured by DLS analysis and found to be about 150 nm, which is similar for all of them. The cytotoxicity of UCNP-PEI and UCNP-PVP is tolerable at a UCNP concentration of 0.25 mg mL^{-1} or less, which is 5 times higher than the concentration used in live-cell imaging. For UCNP-PAA there are no toxicity problems. Considering the surface charges of UCNPs, their cellular uptake behaviours greatly vary and largely determine their cellular uptake efficiency. Positively charged UCNP-PEI significantly enhanced cellular uptake by more than its neutral and negative counterparts, and it has excellent potential for being applied in two-photon induced NIR live-cell imaging and was further engineered as a specific intracellular nanoprobe.

Imaging applications

In this framework the core materials used most are iron oxide,[92–96] and rare and precious metals.[95,97,98] On the other

hand, poly(2-methacryloyloxyethyl(2,3,5-triiodobenzoate)) (polyMAOETIB),[92] starch,[93] metal organic frameworks (MOFs),[94,97] polyethylene glycol,[98] and dextran[96] are used as organic coatings for the shell.

Erathodiyil, N. & Ying, J. Y.[95] reported functionalisation techniques for inorganic nanoparticles used for fluorescence imaging, magnetic resonance imaging (MRI), positron emission tomography (PET) imaging, and multimodal imaging. Numerous types of NPs were used for bioimaging applications, including metal (Au, Ag), metal oxide (Fe_3O_4), and semiconductor nanocrystals (*e.g.* quantum dots (QDs) and magnetic quantum dots (MQDs)) and the most common strategies of engineered NP surfaces consist of physical adsorption or chemisorption of the desired ligands onto the surface. Chemisorption or covalent linkages are favoured while the coated NPs usually possess high colloidal stability, biocompatibility, water solubility, and functional groups for supplementary bioconjugations. In Table 4 a summary of their use and the nature of the core and shell are presented.

Magnetic resonance imaging (MRI)

Metal–organic framework nanoparticles for magnetic resonance imaging have been widely reviewed by Peller, M.[94] Inorganic building units (IBU) based on gadolinium, manganese (^{25}Mn), and iron are mostly used in MOFs for MRI contrast agents.

Galperin, A. & Margel, S. have synthesised and characterised radiopaque magnetic core–shell nanoparticles for magnetic resonance and X-ray imaging applications.[92] The magnetic NPs, consisting of γ-Fe_2O_3/poly(2-methacryloyloxyethyl(2,3,5-triiodobenzoate)) (polyMAOETIB) are prepared by emulsion polymerisation of the iodinated monomer 2-methacryloyloxyethyl(2,3,5-triiodobenzoate) in the presence of maghemite (γ-Fe_2O_3) nanoparticles with a diameter of about 15 nm. The (γ-Fe_2O_3)–polyMAOETIB nanoparticles have a diameter of 56 ± 18 nm. The saturation magnetisation values of the γ-Fe_2O_3 and the core–shell nanoparticles are 66 and 25 emu g^{-1}, respectively. The iodinated monomer on the radiopaque shell that coats the surface of γ-Fe_2O_3 nanoparticles significantly improves the X-ray visibility of the core. The radiopacity of the dried and water dispersed core–shell nanoparticles was demonstrated by an imaging technique based on X-ray absorption usually used in hospitals.

Starch-coated superparamagnetic nanoparticles used as MR contrast agents have been studied by Kim, D. K. *et al.*[93] Superparamagnetic iron oxide nanoparticles (SPION), with a mean size of 6 nm, with polymeric starch were used as organic coatings. The oxidizing agent (H_2O_2) used for the cleavage of the starch's glycosidic bonds influences the particle size: the higher the concentration, the smaller the NP diameter which decreased from 87 nm (0 mg ml^{-1} H_2O_2) to the smallest size of 42 nm (0.092 mg ml^{-1} H_2O_2). Li, Y. *et al.* analysed core–shell upconversion nanoparticle@metal–organic framework nanoprobes for luminescent/magnetic dual-mode targeted imaging.[97] The octagonal nanoparticle consists of the $NaYF_4$:Yb,Er rare-earth-doped upconversion nanoparticle (UCNP) core in an Fe-MIL-101_NH_2 nanoscale metal–organic framework (NMOF) shell, to construct a nanocomposite material for use as an upconversion luminescence (UCL)/MRI tracer. The amino groups on the surface of the NPs are modified with poly(-ethylene glycol)-2-amino ethyl ether acetic acid (NH_2-PEG-COOH) and folic acid (FA), giving PEGylated core–shell UCNP@Fe-MIL-101_NH_2@PEG-FA nanostructures (UMP-FA) that exhibit FA fractions. UMP-FA nanocomposites are tested for UCL/T_2 (type of contrast agent)-MRI dual-mode imaging targeted at KB cells (overexpressing the folate receptor (Fr)) and KB-tumour bearing mice.

Other uses

Devaraj, N. K. *et al.*[96] synthesised cross-linked dextran held together in core–shell formation by a superparamagnetic iron oxide core and functionalised with the radionuclide ^{18}F in high yield *via* "click" chemistry, shown in Fig. 5, for *in vivo* positron emission tomography (PET) imaging. The detection threshold of ^{18}F was 0.025 μg Fe mL^{-1} for PET-CT imaging, approximately 200 times lower than by T2*-weighted MR imaging, so the presence of ^{18}F dramatically lowers the detection limit of the nanoparticles.

Core–shell hybrid nanogels for the integration of optical temperature-sensing, targeted tumour cell imaging and combined chemo-photothermal treatment have been investigated by Wu, W. *et al.*[98] The nanoparticles are formed by coating

Table 4 Imaging applications of core–shell NPs

Core@shell Material	Application	Reference number
γ-Fe_2O_3@poly(2-methacryloyloxyethyl (2,3,5-triiodobenzoate))	Magnetic resonance imaging	92
Fe_3O_4@starch	Magnetic resonance imaging	93
Fe_3O_4@metal–organic framework	Magnetic resonance imaging	94
Metal (Au, Ag) or metal oxide (Fe_3O_4) or semiconductor nanocrystals or magnetic quantum dots@desired ligands	Magnetic resonance imaging, positron emission tomography, and multimodal imaging	95
Fe_3O_4@dextran + radionuclide ^{18}F	*In vivo* positron emission tomography imaging	96
$NaYF_4$:Yb,Er@Fe-MIL-101_NH2	Magnetic resonance imaging	97
Ag–Au@poly(ethylene glycol) + hyaluronic acid chains	Targeted tumour cell imaging and combined chemo-photothermal treatment	98

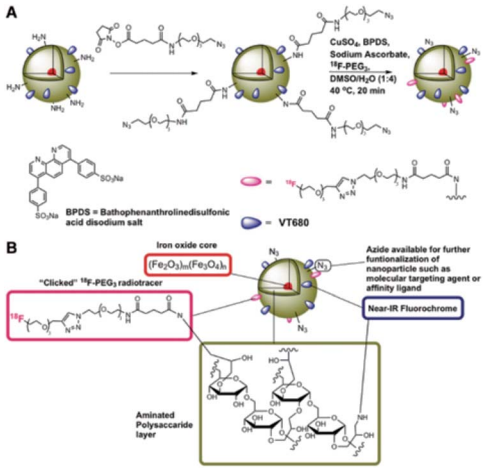

Fig. 5 Preparation of ^{18}F-CLIO; (A) derivatisation of primary amines followed by chemoselective "click" of the ^{18}F-PEG radiotracer; (B) schematic of ^{18}F-CLIO. Reprinted with permission.[96] Copyright 2009 American Chemical Society.

the Ag–Au bimetallic core with a thermo-responsive nonlinear PEG-based hydrogel as the organic shell and using the ligands of hyaluronic acid chains on the surface networks of the gel shell. The Ag–Au core can emit strong visible fluorescence for imaging of mouse melanoma B16F10 cells. The reversible thermoresponsive volume phase transition of the PEG-based gel shell can modify the physicochemical environment of the Ag–Au NP core to manipulate the fluorescence intensity for sensing the environmental temperature alteration, and also offers a high loading capacity for a model anticancer drug (temozolomide) and thermo-triggered drug release. The size is 408 nm.

Application in chemistry and catalysis

The most exploited core materials in this field of application are gold,[99–102] silver,[100,103,104] palladium,[100,102,105–108] platinum,[105] titania[109] and iron oxides.[110–115] In Table 5 a summary of their use and the nature of the core and shell are presented.

Catalytic applications

Thermosensitive Au–polystyrene (PS)–poly(*N*-isopropylacrylamide) (PNIPA) core–shell nanoparticles were studied by Wu, S. *et al.*[99] These NPs use temperature as a reaction trigger. The porosity and hydrophobicity of the coating can be tuned by temperature control while the colloidal stability of the entire structure is maintained. The Au–PNIPA core–shell particles have a diameter of 311 ± 5 nm. The catalytic activity of Au–PNIPA nanoparticles has been measured as a function of temperature T for the reduction of 4-nitrophenol (4-NP) and nitrobenzene (NB), in aqueous solution, respectively. It has been demonstrated that variation of temperature can be used to improve the selectivity of the catalysis for a given substrate; 4-NP reacts much faster at low temperature, while the reduction of NB is preferred at higher temperature. Zhang, W. *et al.*[105] studied a family of metal–organic frameworks with encapsulated noble-metal nanoparticles that exhibit size-selective catalysis. They developed an encapsulation process of noble-metal NPs in MOFs with carboxylic-acid-based ligands, achieving an octahedral crystal shape. These structures have

Table 5 Catalytic applications of core–shell NPs

Core@shell material	Application	Reference number
Au@polystyrene-poly(*N*-isopropylacrylamide)	Thermosensitive reaction trigger	99
Au, Ag or Pd@metallic organic frameworks	Enhancing durability, selectivity, and reactivity of the catalysts and conferring extra functionalities on the catalysts	100
Au–Ni@MIL-101	High activity for hydrogen generation from the catalytic hydrolysis of ammonia borane	102
Ag@metallo-organic	Bonding metal–metal	103
Ag@calcium phosphate and calcium carbonate	Catalyst in the hydration of cyanamides	104
Noble metal@metal organic framework	Size-selective catalysis	105
Pd@metal–organic framework amino-functionalised	Multifunctional catalysts for cascade reactions	106
Pd/ZnO@ZIF-8	Size-selectivity, stability and anti-poisoning in the liquid hydrogenations of alkenes	107
Pd@apricot kernel	Reduction of organic dyes, 4-nitrophenol, methyl orange, methylene blue, rhodamine B, and Congo red	108
TiO_2@carbonaceous type material	Efficient visible light activated photocatalysis	109
Fe_3O_4@sulphonated-phenylacetic acid	Acid magnetic catalyst for the Biginelli reaction	110
Fe_3O_4@piperidine-4-carboxylic acid	Magnetic catalyst but this time for the Knoevenagel reaction	111
Fe_3O_4@3-aminopropyltriethoxysilane + copolymers of acrylic acid and crotonic acid	Removal of cationic dyes from aqueous solution	112
Fe_2O_3@C	Fast and selective removal of oils from a water surface	113
Fe_2O_3@graphene	Adsorbent for organic dyes	114
Metals (Fe, Co, Ni) or alloys (FePt, CoPt) or metal oxides (FeO, Fe_2O_3, Fe_3O_4) or ferrites ($CoFe_2O_4$, $MnFe_2O_4$)@polymer and dendrimer	Versatile supports for catalysts, scavengers, and reagents	115

been employed as novel catalysts in heterogeneous catalysis, in particular for olefin hydrogenation, aqueous reaction in 4-nitrophenol reduction, and enhanced molecular diffusion in CO oxidation. Zamani, F. & Izadi, E.[110] synthesised and characterised sulphonated-phenylacetic acid coated Fe_3O_4 nanoparticles (Fe_3O_4/PAA-SO_3H) as an acid magnetic catalyst for the Biginelli reaction. The nanocomposite has spherical morphology with an average particle size of about 15 nm. The saturation magnetisation values of the samples are 58.7 emu g^{-1} and 68.9 emu g^{-1} for the uncalcined and calcined products respectively. This new acid magnetic catalyst can replace soluble acids with the following advantages: (a) high catalytic activity under mild reaction conditions; (b) easy separation of the catalyst after reaction using an external magnet; (c) reusability of the catalyst for several times. Karaoglu, E. *et al.*[111] also synthesised and characterised nanoparticles for use as a magnetic catalyst but this time for the Knoevenagel reaction. It consists of a piperidine-4-carboxylic acid shell and Fe_3O_4 magnetic core (Fe_3O_4–PPCA). The heterogeneous catalyst exhibited very high conversion rates (97%) and could be recovered easily and reused many times without significant loss of its catalytic activity. The structure has a spherical shape and the average particle size is estimated at 11.2 ± 0.3 nm. The saturation magnetisation value of the sample is 60 emu g^{-1} at 15 kOe. However, this value should be normalised to the weight of the magnetic core. It has been proved that the catalyst is recoverable by magnetic decantation and can be reused several times without significant loss in catalytic activity and selectivity for the Knoevenagel reaction. Kainz, Q. M. and Reiser, O.[115] widely described polymer and dendrimer-coated magnetic nanoparticles as versatile supports for catalysts, scavengers, and reagents. Firstly they described the synthesis and strategies of surface functionalisation of the most common superparamagnetic iron oxide nanoparticles (SPIONs) derived from metals (Fe, Co, Ni), alloys (FePt, CoPt), metal oxides (FeO, Fe_2O_3, Fe_3O_4), and ferrites ($CoFe_2O_4$, $MnFe_2O_4$). Then they explained how the boosting action of dendrimers and polymers attached to the surface of the nanomagnets works, enhancing the loading capacity with their functional groups either by ligation with previously synthesized dendrimers or polymers or by surface-initiated synthesis. The ligation permits the attachment of commercial materials and the synthesis on the particles supports functionalisation and tuning of the properties. The as-formed core–shell hybrid materials are extensively used as recyclable platforms for organic chemistry, for example in the extraction of analytes or contaminants, as supports for metal and organocatalysts, and in the formulation of magnetic scavengers and reagents. Metal organic frameworks (MOFs) are widely used as shells for core–shell nanoparticles in catalytic applications. To give some examples, the studies of Zhao, M. *et al.*,[106] Lin, L. *et al.*,[107] Gu, X. *et al.*[102] and Hu, P. *et al.*[100] are presented. The first paper sees core–shell palladium nanoparticle@metal–organic frameworks as multifunctional catalysts for cascade reactions. Pd core nanoparticles, coated with an amino-functionalised IRMOF-3 shell, are prepared by a facile mixed solvothermal method. The average diameters are between 326 nm and 341 nm. The nanostructures show high activity, enhanced selectivity and stability in the cascade reaction. In the second paper the researchers synthesised Pd/ZnO@ZIF-8 core–shell microspheres. The synthesis method first involves loading Pd nanoparticles onto the surface of the ZnO microsphere to form a Pd/ZnO core and then coating the core with a layer of defect-free ZIF-8. The average thickness of the outer ZIF-8 shell is around 95 nm and the diameter of the inner Pd/ZnO core is about 350 nm. The structure exhibited excellent performance in terms of size-selectivity, stability and anti-poisoning in the liquid hydrogenation of alkenes.

The third paper explains how Au–Ni alloy nanoparticles are successfully coated with MIL-101, with size and location control, through the double solvents method (DSM) combined with a liquid-phase concentration-controlled reduction strategy. NPs inside the mesoporous MIL-101 exhibit high activity for hydrogen generation from the catalytic hydrolysis of ammonia borane. By varying the concentration of the $NaBH_4$ reductant solution, AuNi@MIL-101_b NPs change their size from 2.0–5.0 nm (0.4 M $NaBH_4$) to diameters greater than 5.0 nm (0.2 M NaBH4).

In the last cited work the researchers wrote an overview regarding the encapsulation of well-defined nanoparticle catalysts, such as Au, Ag and Pd in metallic organic frameworks (MOFs) to form a core–shell nanostructure which can enhance the durability, selectivity, and reactivity of the catalysts and confer extra functionalities on the catalysts.

Wastewater treatment applications

Khodadadi, B. *et al.*[108] reported a green synthesis of Pd nanoparticles in an apricot kernel shell substrate using *Salvia hydrangea* extract as an organic reducing agent and proved their catalytic activity for reduction of organic dyes, 4-nitrophenol (4-NP), methyl orange (MO), methylene blue (MB), rhodamine B (RhB), and Congo Red (CR) at room temperature. In addition, it was found that the Pd NPs/Apricot kernel shell can be recovered and reused several times without significant loss of catalytic activity. The synthesis procedure is presented in Fig. 6. Moustakas, N. G. *et al.*[109] have synthesised inorganic–organic core–shell titania nanoparticles for efficient visible light activated photocatalysis. The modified TiO_2 (m-TiO_2) nanostructure covered with a shell of carbonaceous type material, which acts as a highly efficient visible light sensitiser, was synthesised using the gel combustion method. The photocatalytic

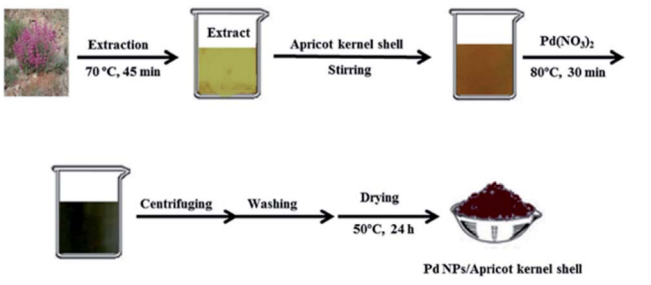

Fig. 6 Synthesis procedure of Pd NPs/Apricot kernel shell. Reprinted with permission from Elsevier.[108]

performance of the m-TiO_2 powder was tested for the degradation of methylene blue (MB) azo dye under UVA (350–365 nm), visible (440–460 nm) and daylight (350–750 nm) illumination. The visible light activation of the material is due to the formation of monolayers of carbonaceous species which cover the TiO_2 core anatase nanoparticles. The particles size is 3–10 nm.

Ge, F. *et al.*[112] have found an efficient method for removing cationic dyes from aqueous solution using polymer-modified magnetic nanoparticles. The magnetic nanoparticles (MNPs) modified with 3-aminopropyltriethoxysilane and copolymers of acrylic acid and crotonic acid are proved to remove cationic dyes such as crystal violet, methylene blue and alkali blue 6B, from water solution by adsorption. The NPs demonstrated high efficiency as a reusable adsorbent for fast removal of cationic dyes from aqueous solution.

Zhu, Q. *et al.*[113] have investigated a fast and selective removal of oils from a water surface *via* highly hydrophobic core–shell Fe_2O_3@C nanoparticles with hydrophobic polysiloxane layers, as shown in Fig. 7, in a magnetic field. The particles exhibit highly hydrophobic and super oleophilic properties and can selectively absorb lubricating oil up to 3.8 times the particle weight while completely repelling water. The NPs which absorbed oil are rapidly collected in a few seconds through the application of an external magnetic field. It is then possible to remove the oil from the surfaces of nanoparticles using a simple ultrasonic treatment. The particle size fluctuates between 30 and 200 nm.

Fan, W. *et al.*[114] engineered graphene sheets and carbon-coated Fe_3O_4 nanoparticles as a synergistic adsorbent of organic dyes. Magnetic graphene–Fe_3O_4@carbon (GFC) nanostructures were firstly prepared *via* a one-pot solvothermal process; carbonaceous coatings were then applied on Fe_3O_4 nanoparticles synthesised through a hydrothermal carbonisation process using glucose as a carbon source. Graphene sheets successfully prevent the Fe_3O_4 nanoparticles from aggregating and facilitate a good dispersion of the magnetic nanoparticles. The carbonaceous layer shields the Fe_3O_4 nanoparticles in acidic environments and improves the specific surface area of the nanostructure which is crucial for the removal of organic dyes, such as methylene blue (MB). The adsorption properties are demonstrated in water and in acidic environments, and about 86% and 77% of the dye removal efficiency can be maintained after five adsorption–desorption cycles in water and 1 M HCl, respectively. The adsorption capacity was found to be about 40% higher compared with the corresponding binary graphene–Fe_3O_4 and Fe_3O_4@carbon hybrids. TEM analysis revealed that the as-formed particle has a core–shell structure with an Fe_3O_4 core and a carbonaceous shell having an average thickness of about 15 nm. The specific saturation magnetisation value is 74.2 emu g^{-1} for Fe_3O_4, 42.2 emu g^{-1} for the graphene–Fe_3O_4 hybrid and 19.1 emu g^{-1} for the GFC hybrid. For the latter, the reduction in the value of magnetisation could be due to the lower amount of Fe_3O_4, which is estimated to be 45 wt%.

Other applications

Ide, E. *et al.*[103] proposed a novel bonding metal–metal process catalysed by Ag@metallo-organic nanoparticles. The removal of the organic shell is necessary to bring out the capacities of the nanoparticles, and it takes place through an oxidation reaction. Its decomposition temperature measured by thermal analysis is 573 K. At a low bonding temperature of 573 K and a bonding pressure of 1 or 5 MPa, Cu-to-Cu bonding using the silver nanoparticles is achieved. The shear strength of the joints is 25–40 MPa. Momeni, S. S. *et al.*[104] have proposed a biosynthesis of the Ag/bone (calcium phosphate and calcium carbonate) nanocomposite for the hydration of cyanamides in *Myrica gale* L. extract to be used as a green solvent. The *Myrica gale* L. aqueous extract acts as a reducing and stabilising agent in the synthesis and as a catalyst in the hydration of cyanamides under environmentally gentle reaction conditions in the aqueous extract as a green solvent without use of toxic and harmful chemicals.

This method does not require any purification techniques since no by-product is formed and the catalyst can be easily recovered and reused. After the hydration reaction of 4-chlorophenylcyanamide has reached completion, the catalyst is separated and is washed with ethanol, and dried in a hot air oven at 100 °C for 2 h and the recycled catalyst is saved for the next reaction. The recycled catalyst can be reused five times with no loss of activity, as shown in Fig. 8.

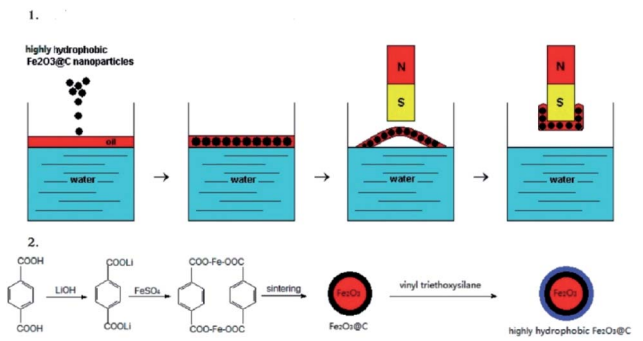

Fig. 7 Illustration of (1) oil removal from the water surface and (2) the preparation of the NPs. Reprinted with permission.[113] Copyright 2010 American Chemical Society.

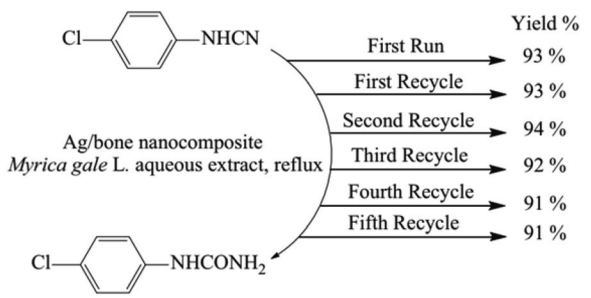

Fig. 8 Reusability of the Ag/bone nanocomposite for the hydration of 4-chlorophenylcyanamide. Reprinted with permission from Elsevier.[104]

Conclusions

This review reports many novel applications from the field of nanoscale structures and shows how many types of material combinations are extensively studied and enhanced for useful applications, ranging from electrical, drug delivery, biomedical, and imaging to catalysis. The efficiency of a core/shell conductive nanoparticle can be improved or tuned by means of the coating material or its thickness which changes the magnetic core surface anisotropy. In drug delivery studies it is important to stress that what it is being investigated most is the possibility of tuning the core or shell release by varying the pH or temperature conditions which influence the molecular links and structures of the materials used. In the biomedical field instead, the most sought after feature is biocompatibility and the ease of disposal of the substances used by the human body, something that is required in magnetic resonance imaging applications too. An important quest that pervades the catalysis branch is the regeneration efficiency and the environmental friendliness of the catalyst studied in conjunction with the conditions of use that are increasingly required to be mild and as less toxic as possible. Given the wide breakthrough discoveries of the last two decades, in the future we can surely expect new discoveries that will exhibit many new properties and bring improvement in the properties, synthesis, and applications of this class of nanomaterials in constant evolution.

Conflicts of interest

There are no conflicts to declare.

Acknowledgements

This study was supported by Fondazione Cariplo (project REVENUE).

Notes and references

1 G. Liu, M. Swierczewska, S. Lee and X. Chen, *Nano Today*, 2010, **5**, 524–539.
2 H. L. Liu, P. Hou, W. X. Zhang and J. H. Wu, *Colloid. Surface. Physicochem. Eng. Aspect.*, 2010, **356**, 21–27.
3 C. F. Hoener, K. A. Allan, A. J. Bard, A. Campion, M. A. Fox, T. E. Mallouk, S. E. Webber and J. M. White, *J. Phys. Chem.*, 1992, **96**, 3812–3817.
4 I. Honma, T. Sano and H. Komiyama, *J. Phys. Chem.*, 1993, **97**, 6692–6695.
5 H. S. Zhou, H. Sasahara, I. Honma, H. Komiyama and J. W. Haus, *Chem. Mater.*, 1994, **6**, 1534–1541.
6 J. Ahmed, S. Sharma, K. V. Ramanujachary, S. E. Lofland and A. K. Ganguli, *J. Colloid Interface Sci.*, 2009, **336**, 814–819.
7 S. A. El-Safty, *J. Colloid Interface Sci.*, 2008, **319**, 477–488.
8 Z. Ji, X. Shen, G. Zhu, H. Zhou and A. Yuan, *J. Mater. Chem.*, 2012, **22**, 3471–3477.
9 G. Salazar-Alvarez, J. Qin, V. Šepelák, I. Bergmann, M. Vasilakaki, K. N. Trohidou, J. D. Ardisson, W. A. A. Macedo, M. Mikhaylova, M. Muhammed, M. D. Baró and J. Nogués, *J. Am. Chem. Soc.*, 2008, **130**, 13234–13239.
10 E. Schmidt, A. Vargas, T. Mallat and A. Baiker, *J. Am. Chem. Soc.*, 2009, **131**, 12358–12367.
11 Q. Song and Z. J. Zhang, *J. Am. Chem. Soc.*, 2004, **126**, 6164–6168.
12 Z. L. Wang, T. S. Ahmad and M. A. El-Sayed, *Surf. Sci.*, 1997, **380**, 302–310.
13 M. Yamada, S. Kon and M. Miyake, *Chem. Lett.*, 2005, **34**, 1050–1051.
14 J. S. Hu, Y. G. Guo, H. P. Liang, L. J. Wan and L. Jiang, *J. Am. Chem. Soc.*, 2005, **127**, 17090–17095.
15 M. Jitianu and D. V. Goia, *J. Colloid Interface Sci.*, 2007, **309**, 78–85.
16 N. J. Suematsu, Y. Ogawa, Y. Yamamoto and T. Yamaguchi, *J. Colloid Interface Sci.*, 2007, **310**, 648–652.
17 T. Z. Ren, Z. Y. Yuan, W. Hu and X. Zou, *Microporous Mesoporous Mater.*, 2008, **112**, 467–473.
18 L. Wu, J. C. Yu, L. Zhang, X. Wang and S. Li, *J. Solid State Chem.*, 2004, **177**, 3666–3674.
19 X. Qu, L. Omar, T. B. H. Le, L. Tetley, K. Bolton, K. W. Chooi, W. Wang and I. F. Uchegbu, *Langmuir*, 2008, **24**, 9997–10004.
20 G. Cao and D. Liu, *Adv. Colloid Interface Sci.*, 2008, **136**, 45–64.
21 K. B. Shelimov and M. Moskovits, *Chem. Mater.*, 2000, **12**, 250–254.
22 R. Xiao, I. C. Seung, R. Liu and B. L. Sang, *J. Am. Chem. Soc.*, 2007, **129**, 4483–4489.
23 T. Y. Shin, S. H. Yoo and S. Park, *Chem. Mater.*, 2008, **20**, 5682–5686.
24 J. A. Sioss and C. D. Keating, *Nano Lett.*, 2005, **5**, 1779–1783.
25 Z. Liu, D. Elbert, C. L. Chien and P. C. Searson, *Nano Lett.*, 2008, **8**, 2166–2170.
26 X. Wendy Gu, N. Shadmi, T. S. Yarden, H. Cohen and E. Joselevich, *J. Phys. Chem. C*, 2012, **116**, 20121–20126.
27 Y. Wu, T. Livneh, Y. X. Zhang, G. Cheng, J. Wang, J. Tang, M. Moskovits and G. D. Stucky, *Nano Lett.*, 2004, **4**, 2337–2342.
28 M. Li, T. S. Mayer, J. A. Sioss, C. D. Keating and R. B. Bhiladvala, *Nano Lett.*, 2007, **7**, 3281–3284.
29 R. Narayanan and M. A. El-Sayed, *J. Phys. Chem. B*, 2004, **108**, 5726–5733.
30 Z. H. Lu and Q. Xu, *J. Chem. Phys.*, 2011, **134**, 034305.
31 H. Lee, S. E. Habas, S. Kweskin, D. Butcher, G. A. Somorjai and P. Yang, *Angew. Chem., Int. Ed.*, 2006, **45**, 7824–7828.
32 J. E. Millstone, S. J. Hurst, G. S. Métraux, J. I. Cutler and C. A. Mirkin, *Small*, 2009, **5**, 646–664.
33 D. Williams and I. Sebastine, *IEE Proc.: Nanobiotechnol.*, 2005, **152**, 207–211.
34 C. M. Lieber, *Solid State Commun.*, 1998, **107**, 607–616.
35 R. E. Smalley and B. I. Yakobson, *Solid State Commun.*, 1998, **107**, 597–606.
36 J. Chen, T. Herricks and Y. Xia, *Angew. Chem., Int. Ed.*, 2005, **44**, 2589–2592.

37 S. J. Oldenburg, R. D. Averitt, S. L. Westcott and N. J. Halas, *Chem. Phys. Lett.*, 1998, **288**, 243–247.
38 N. Sounderya and Y. Zhang, *Recent Pat. Biomed. Eng.*, 2010, **1**, 34–42.
39 M. J. Kim, Y. H. Choa, D. H. Kim and K. H. Kim, *IEEE Trans. Magn.*, 2009, **45**, 2446–2449.
40 S. Laurent, D. Forge, M. Port, A. Roch, C. Robic, L. Vander Elst and R. N. Muller, *Chem. Rev.*, 2008, **108**, 2064–2110.
41 V. Salgueiriño-Maceira and M. A. Correa-Duarte, *Adv. Mater.*, 2007, **19**, 4131–4144.
42 M. C. Daniel and D. Astruc, *Chem. Rev.*, 2004, **104**, 293–346.
43 J. Xu, F. Zeng, S. Wu, X. Liu, C. Hou and Z. Tong, *Nanotechnology*, 2007, **18**, 26.
44 L. Qi, J. Ma, H. Cheng and Z. Zhao, *Colloid. Surface. Physicochem. Eng. Aspect.*, 1996, **111**, 195–202.
45 L. Babes, J. Jacques, L. Jeune and P. Jallet, *J. Colloid Interface Sci.*, 1999, **482**, 474–482.
46 J. P. Zimmer, S. W. Kim, S. Ohnishi, E. Tanaka, J. V. Frangioni and M. G. Bawendi, *J. Am. Chem. Soc.*, 2006, **128**, 2526–2527.
47 A. K. Gupta and M. Gupta, *Biomaterials*, 2005, **26**, 3995–4021.
48 P. M. A. De Farias, B. S. Santos, F. D. Menezes, A. G. Brasil, R. Ferreira, M. A. Motta, A. G. Castro-Neto, A. A. S. Vieira, D. C. N. Silva, A. Fontes and C. L. Cesar, *Appl. Phys. Mater. Sci. Process*, 2007, **89**, 957–961.
49 E. Yan, Y. Ding, C. Chen, R. Li, Y. Hu and X. Jiang, *Chem. Commun.*, 2009, 2718–2720.
50 P. A. Dresco, V. S. Zaitsev, R. J. Gambino and B. Chu, *Langmuir*, 1999, **15**, 1945–1951.
51 J. Deng, C. L. He, Y. Peng, J. Wang, X. Long, P. Li and A. S. C. Chan, *Synth. Met.*, 2003, **139**, 295–301.
52 N. A. D. Burke, H. D. H. Stöver and F. P. Dawson, *Chem. Mater.*, 2002, **14**, 4752–4761.
53 C. R. Vestal and Z. J. Zhang, *J. Am. Chem. Soc.*, 2002, **124**, 14312–14313.
54 A. Maliakal, H. Katz, P. M. Cotts, S. Subramoney and P. Mirau, *J. Am. Chem. Soc.*, 2005, **127**, 14655–14662.
55 D. J. S. Balamurugan Balasubramanian, K. L. Kraemer, N. A. Reding, R. Skomski and S. Ducharme, *ACS Nano*, 2010, **4**, 1893–1900.
56 Z. Du, X. Yin, M. Zhang, Q. Hao, Y. Wang and T. Wang, *Mater. Lett.*, 2010, **64**, 2076–2079.
57 T. R. Dhakal, S. R. Mishra, Z. Glenn and B. K. Rai, *J. Nanosci. Nanotechnol.*, 2012, **12**, 6389–6396.
58 S. Wu, *J. Mater. Sci. Mater. Electron.*, 2007, **18**, 447–452.
59 T. Kim, H. Kang, S. Jeong, D. J. Kang, C. Lee, C. H. Lee, M. K. Seo, J. Y. Lee and B. J. Kim, *ACS Appl. Mater. Interfaces*, 2014, **6**, 16956–16965.
60 H. Chen, W. Dong, J. Ge, C. Wang, X. Wu, W. Lu and L. Chen, *Sci. Rep.*, 2013, **3**, 1–6.
61 L. Xie, X. Huang, Y. Huang, K. Yang and P. Jiang, *J. Phys. Chem. C*, 2013, **117**, 22525–22537.
62 P. Liu, *Colloid. Surface. Physicochem. Eng. Aspect.*, 2006, **291**, 155–161.
63 S. Chen, Y. Li, C. Guo, J. Wang, J. Ma, X. Liangs, L. R. Yang and H. Z. Liu, *Langmuir*, 2007, **23**, 12669–12676.
64 X. Liu, M. D. Kaminski, H. Chen, M. Torno, L. T. Taylor and A. J. Rosengart, *J. Controlled Release*, 2007, **119**, 52–58.
65 R. Liu, Y. Guo, G. Odusote, F. Qu and R. D. Priestley, *ACS Appl. Mater. Interfaces*, 2013, **5**, 9167–9171.
66 M. Rahimi, A. Wadajkar, K. Subramanian, M. Yousef, W. Cui, J. T. Hsieh and K. T. Nguyen, *Nanomed. Nanotechnol. Biol. Med.*, 2010, **6**, 672–680.
67 J. M. Chem, B. Chang, X. Sha, J. Guo, Y. Jiao and W. Yang, *J. Mater. Chem.*, 2011, 9239–9247.
68 L. Xing, H. Zheng, Y. Cao and S. Che, *Adv. Mater.*, 2012, **24**, 6433–6437.
69 S.-G. Zhu, J.-J. Xiang, X.-L. Li, S.-R. Shen, H. Lu, J. Zhou, W. Xiong, B.-C. Zhang, X.-M. Nie, M. Zhou, K. Tang and G.-Y. Li, *Biotechnol. Appl. Biochem.*, 2004, **39**, 179.
70 T. Borase, M. Iacono, S. I. Ali, P. D. Thornton and A. Heise, *Polym. Chem.*, 2012, **3**, 1267–1275.
71 A. Popat, J. Liu, G. Q. Lu and S. Z. Qiao, *J. Mater. Chem.*, 2012, **22**, 11173–11178.
72 H. Otsuka, Y. Nagasaki and K. Kataoka, *Adv. Drug Deliv. Rev.*, 2003, **55**, 403–419.
73 K. Deng, Z. Hou, X. Li, C. Li, Y. Zhang, X. Deng, Z. Cheng and J. Lin, *Sci. Rep.*, 2015, **5**, 1–7.
74 Z. Y. Zhang, Y. D. Xu, Y. Y. Ma, L. L. Qiu, Y. Wang, J. L. Kong and H. M. Xiong, *Angew. Chem., Int. Ed.*, 2013, **52**, 4127–4131.
75 S. Qin, L. Wang, X. Zhang and G. Su, *Appl. Surf. Sci.*, 2010, **257**, 731–735.
76 D. L. Zhao, P. Teng, Y. Xu, Q. S. Xia and J. T. Tang, *J. Alloys Compd.*, 2010, **502**, 392–395.
77 C. C. Berry, S. Wells, S. Charles and A. S. G. Curtis, *Biomaterials*, 2003, **24**, 4551–4557.
78 O. Ziv, R. R. Avtalion and S. Margel, *J. Biomed. Mater. Res.*, 2008, **85**, 1011–1021.
79 L. D. Tran, N. M. T. Hoang, T. T. Mai, H. V. Tran, N. T. Nguyen, T. D. Tran, M. H. Do, Q. T. Nguyen, D. G. Pham, T. P. Ha, H. Van Le and P. X. Nguyen, *Colloid. Surface. Physicochem. Eng. Aspect.*, 2010, **371**, 104–112.
80 L. Zhou, J. Yuan and Y. Wei, *J. Mater. Chem.*, 2011, **21**, 2823–2840.
81 S. Rana, N. V. Jadhav, K. C. Barick, B. N. Pandey and P. A. Hassan, *Dalton Trans.*, 2014, **43**, 12263–12271.
82 H. Xu, Z. P. Aguilar, L. Yang, M. Kuang, H. Duan, Y. Xiong, H. Wei and A. Wang, *Biomaterials*, 2011, **32**, 9758–9765.
83 W. H. Zhou, C. H. Lu, X. C. Guo, F. R. Chen, H. H. Yang and X. R. Wang, *J. Mater. Chem.*, 2010, **20**, 880–883.
84 U. C. Palmiero, A. M. Küffner, F. Krumeich, L. Faltova and P. Arosio, *Angew. Chem., Int. Ed.*, 2020, **59**, 8138–8142.
85 Y. Xian, Y. Hu, F. Liu, Y. Xian, H. Wang and L. Jin, *Biosens. Bioelectron.*, 2006, **21**, 1996–2000.
86 D. Hühn, K. Kantner, C. Geidel, S. Brandholt, I. De Cock, S. J. H. Soenen, P. Riveragil, J. M. Montenegro, K. Braeckmans, K. Müllen, G. U. Nienhaus, M. Klapper and W. J. Parak, *ACS Nano*, 2013, **7**, 3253–3263.
87 R. Marega, L. Karmani, L. Flamant, P. G. Nageswaran, V. Valembois, B. Masereel, O. Feron, T. Vander Borght,

S. Lucas, C. Michiels, B. Gallez and D. Bonifazi, *J. Mater. Chem.*, 2012, **22**, 21305–21312.
88 R. Chen, J. Zhang, Y. Wang, X. Chen, J. A. Zapien and C. S. Lee, *Nanoscale*, 2015, **7**, 17299–17305.
89 A. Dong, J. Huang, S. Lan, T. Wang, L. Xiao, W. Wang, T. Zhao, X. Zheng, F. Liu, G. Gao and Y. Chen, *Nanotechnology*, 2011, **22**, 29.
90 J. Jin, Y. J. Gu, C. W. Y. Man, J. Cheng, Z. Xu, Y. Zhang, H. Wang, V. H. Y. Lee, S. H. Cheng and W. T. Wong, *ACS Nano*, 2011, **5**, 7838–7847.
91 H. S. Choi, W. Liu, F. Liu, K. Nasr, P. Misra, M. G. Bawendi and J. V. Frangioni, *Nat. Nanotechnol.*, 2010, **5**, 42–47.
92 A. Galperin and S. Margel, *J. Biomed. Mater. Res. B Appl. Biomater.*, 2007, **83**, 490–498.
93 D. K. Kim, M. Mikhaylova, F. H. Wang, J. Kehr, B. Bjelke, Y. Zhang, T. Tsakalakos and M. Muhammed, *Chem. Mater.*, 2003, **15**, 4343–4351.
94 M. Peller, K. Böll, A. Zimpel and S. Wuttke, *Inorg. Chem. Front.*, 2018, **5**, 1760–1779.
95 N. Erathodiyil and J. Y. Ying, *Acc. Chem. Res.*, 2011, **44**, 925–935.
96 N. K. Devaraj, E. J. Keliher, G. M. Thurber, M. Nahrendorf and R. Weissleder, *Bioconjugate Chem.*, 2009, **20**, 397–401.
97 Y. Li, J. Tang, L. He, Y. Liu, Y. Liu, C. Chen and Z. Tang, *Adv. Mater.*, 2015, **27**, 4075–4080.
98 W. Wu, J. Shen, P. Banerjee and S. Zhou, *Biomaterials*, 2010, **31**, 7555–7566.
99 S. Wu, J. Dzubiella, J. Kaiser, M. Drechsler, X. Guo, M. Ballauff and Y. Lu, *Angew. Chem., Int. Ed.*, 2012, **51**, 2229–2233.
100 P. Hu, J. V. Morabito and C. K. Tsung, *ACS Catal.*, 2014, **4**, 4409–4419.
101 Q. L. Zhu, J. Li and Q. Xu, *J. Am. Chem. Soc.*, 2013, **135**, 10210–10213.
102 X. Gu, Z. H. Lu, H. L. Jiang, T. Akita and Q. Xu, *J. Am. Chem. Soc.*, 2011, **133**, 11822–11825.
103 E. Ide, S. Angata, A. Hirose and K. F. Kobayashi, *Acta Mater.*, 2005, **53**, 2385–2393.
104 S. S. Momeni, M. Nasrollahzadeh and A. Rustaiyan, *J. Colloid Interface Sci.*, 2017, **499**, 93–101.
105 W. Zhang, G. Lu, C. Cui, Y. Liu, S. Li, W. Yan, C. Xing, Y. R. Chi, Y. Yang and F. Huo, *Adv. Mater.*, 2014, **26**, 4056–4060.
106 M. Zhao, K. Deng, L. He, Y. Liu, G. Li, H. Zhao and Z. Tang, *J. Am. Chem. Soc.*, 2014, **136**, 1738–1741.
107 L. Lin, T. Zhang, H. Liu, J. Qiu and X. Zhang, *Nanoscale*, 2015, **7**, 7615–7623.
108 B. Khodadadi, M. Bordbar and M. Nasrollahzadeh, *J. Colloid Interface Sci.*, 2017, **490**, 1–10.
109 N. G. Moustakas, A. G. Kontos, V. Likodimos, F. Katsaros, N. Boukos, D. Tsoutsou, A. Dimoulas, G. E. Romanos, D. D. Dionysiou and P. Falaras, *Appl. Catal. B Environ.*, 2013, **130–131**, 14–24.
110 F. Zamani and E. Izadi, *Catal. Commun.*, 2013, **42**, 104–108.
111 E. Karaoglu, A. Baykal, M. Şenel, H. Sözeri and M. S. Toprak, *Mater. Res. Bull.*, 2012, **47**, 2480–2486.
112 F. Ge, H. Ye, M. M. Li and B. X. Zhao, *Chem. Eng. J.*, 2012, **198–199**, 11–17.
113 Q. Zhu, F. Tao and Q. Pan, *ACS Appl. Mater. Interfaces*, 2010, **2**, 3141–3146.
114 W. Fan, W. Gao, C. Zhang, W. W. Tjiu, J. Pan and T. Liu, *J. Mater. Chem.*, 2012, **22**, 25108–25115.
115 Q. M. Kainz and O. Reiser, *Acc. Chem. Res.*, 2014, **47**, 667–677.